

RSC Advances



This is an *Accepted Manuscript*, which has been through the Royal Society of Chemistry peer review process and has been accepted for publication.

Accepted Manuscripts are published online shortly after acceptance, before technical editing, formatting and proof reading. Using this free service, authors can make their results available to the community, in citable form, before we publish the edited article. This *Accepted Manuscript* will be replaced by the edited, formatted and paginated article as soon as this is available.

You can find more information about *Accepted Manuscripts* in the [Information for Authors](#).

Please note that technical editing may introduce minor changes to the text and/or graphics, which may alter content. The journal's standard [Terms & Conditions](#) and the [Ethical guidelines](#) still apply. In no event shall the Royal Society of Chemistry be held responsible for any errors or omissions in this *Accepted Manuscript* or any consequences arising from the use of any information it contains.

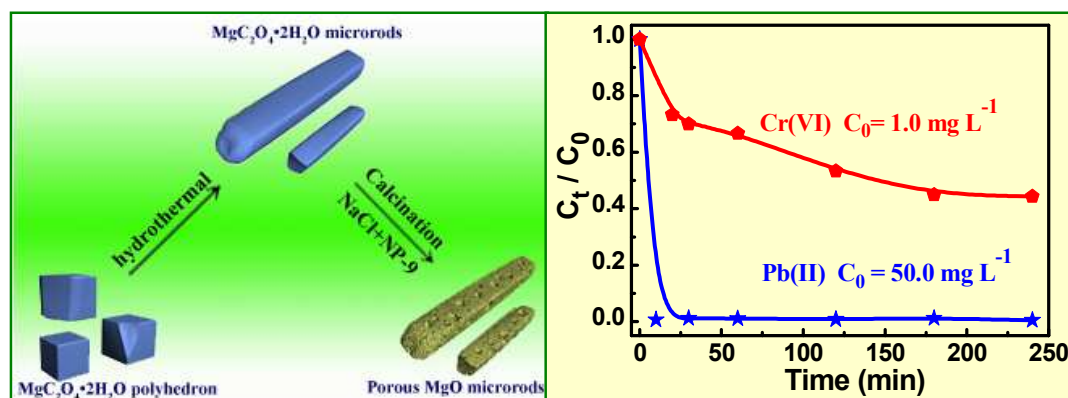
Graphical abstract for:

Hydrothermal-thermal conversion synthesis of hierarchical porous MgO microrods as efficient adsorbents for lead (II) and chromium (VI) removal

Linlin Zhang¹, Wancheng Zhu^{1,*}, Heng Zhang¹, Siwei Bi¹, Qiang Zhang^{2,*}

1. Department of Chemical Engineering, Qufu Normal University, Shandong 273165, China
2. Department of Chemical Engineering, Tsinghua University, Beijing 100084, China

High crystallinity porous MgO microrods were synthesized *via* a NaCl and NP-9 assisted calcination of the hydrothermally synthesized $\text{MgC}_2\text{O}_4 \cdot 2\text{H}_2\text{O}$ microrods, which exhibited satisfactory removal efficiency for Pb (II) and Cr (VI) ions from aqueous solutions.



* Corresponding authors. Tel.: +86-537-4453130.

Email: zhuwancheng@tsinghua.org.cn
zhang-qiang@mails.tsinghua.edu.cn (Q. Zhang).

(W.C. Zhu);

Hydrothermal-thermal conversion synthesis of hierarchical porous MgO microrods as efficient adsorbents for lead (II) and chromium (VI) removal

Linlin Zhang¹, Wancheng Zhu^{1,*}, Heng Zhang¹, Siwei Bi¹, Qiang Zhang^{2,*}

1. Department of Chemical Engineering, Qufu Normal University, Shandong 273165, China

2. Beijing Key Laboratory of Green Chemical Reaction Engineering and Technology, Department of Chemical Engineering, Tsinghua University, Beijing 100084, China

Abstract:

High crystallinity magnesium oxide (MgO) microrods with hierarchical porous structure (ranging from micropores to mesopores and macropores) and well-defined rod-like morphology have been successfully synthesized *via* a flux NaCl and surfactant nonyl phenol polyoxyethylene ether (NP-9) directed thermal decomposition of the hydrothermally derived magnesium oxalate dihydrate ($\text{MgC}_2\text{O}_4 \cdot 2\text{H}_2\text{O}$) microrods. The successive and synergistic effect of NaCl and NP-9 assisted the thermal conversion and promoted the final formation of the well-defined porous MgO microrods with a specific surface area of $50.2 \text{ m}^2 \text{ g}^{-1}$ and well preserved rod-like morphology of the $\text{MgC}_2\text{O}_4 \cdot 2\text{H}_2\text{O}$ precursor. The as-obtained porous MgO microrods were employed as efficient adsorbents for removal of heavy metal ions such as Pb (II) and Cr (VI) from aqueous solutions, and the removal efficiency of Pb (II) (original concentration: 50.0 mg L^{-1}) and Cr (VI) (original concentration: 1.0 mg L^{-1}) was up to 99.5 % and 55.6 %, respectively. Such well-defined MgO microrods with hierarchical porous structure can also serve as promising candidates for catalyst support and even catalyst itself in addition to the present waste water treatment in various fields.

Key words: magnesium oxide; porous; rod-like; hydrothermal; thermal conversion; adsorbent

* Corresponding authors. Tel.: +86-537-4453130.

Email: zhuwancheng@tsinghua.org.cn (W.C. Zhu); zhang-qiang@mails.tsinghua.edu.cn (Q. Zhang).

1. Introduction

The porous metal oxides have been extensively investigated recently owing to their great potential applications in catalysis, adsorption and separation, as well as energy conversion and storage¹⁻³ due to their extraordinary characteristics, such as high surface area, high pore volume, well-defined morphology, and structural flexibility^{4,5}. Particularly, porous metal oxides with three-dimensional (3D) hierarchical architectures, such as MgO^{6,7}, Al₂O₃⁸, NiO⁹, ZnO¹⁰⁻¹², Fe₂O₃^{13,14}, Fe₃O₄¹⁵, and TiO₂¹⁶, assembled by one-dimensional (1D) nanostructures have attracted more and more attention owing to their unique structures and properties¹³. The nanometer-sized building blocks interacted with overall micrometer-sized structures exhibit small size effect as well as desirable mechanical strength, easy recovery, and facile transportation⁷.

Among numerous metal oxides, magnesium oxide (MgO) has strongly been considered. As an important inorganic compound, MgO has been widely used as ceramic¹⁷ and refractory¹⁸ material. In addition, MgO has also been employed as catalyst support for carbon nanotube growth^{19,20}, catalyst for transesterification²¹, and adsorbents for wastewater treatment^{22,23}, for its distinct advantages such as low cost, and environmental friendliness. Most recently, groundwater contamination by heavy metals and dyes has been a rising worldwide environmental concerns due to its high toxicity to human beings, animals, and environment²⁴⁻²⁸. In all efforts toward such concern, MgO has shown excellent adsorption abilities in wastewater treatment for its high surface reactivity and destructive sorbent²⁹. Venkatesha et al. synthesized MgO nanoparticles (NPs) and employed them for adsorption of reactive and vat dyes, and the maximum adsorption capacities for Levafix Fast Red CA (LFR) and Indanthren Blue BC (IB) were 92.2 and 86.5 mg g⁻¹, respectively²⁹. Cao et al. obtained flowerlike MgO nanostructures *via* microwave assisted solvothermal method, which showed superb adsorption capacities for Pb (II) and Cd (II)³⁰.

Up to now, many synthetic routes have been developed to synthesize porous MgO structures, such as hydrothermal method^{31,32}, pulsed-laser deposition³³, *in situ* chemical vapor deposition^{5,6} and thermal decomposition of magnesium salts^{34,35}, or magnesium hydroxide³⁶⁻³⁸. Yu et al.³⁶

obtained worm-like porous MgO nanoplates through the calcination of the hydrothermally synthesized $\text{Mg}(\text{OH})_2$ precursor. Mesoporous MgO microspheres were acquired by calcination of MgCO_3 at 500 °C for 3.0 h, containing three levels (small mesopores, large mesopores and macropores) of hierarchical porous organization ³⁹. Very recently, we have just successfully synthesized hierarchical porous MgO superstructures with a well faceted polyhedron-like profile *via* a coprecipitation process followed by a facile flux and surfactant directed decomposition ⁴⁰. However, taking the facile treatments and rational applications into consideration, it is still a challenge to obtain porous MgO nanostructures of high crystallinity with controllable and well-defined 3D hierarchical morphology and porosity.

In this contribution, high crystallinity porous microrods of MgO were synthesized by a facile hydrothermal-thermal conversion process, in which MgO retained the 1D rod-like morphological feature of the precursor during the thermal conversion. Since the thermal decomposition was free of NO_x and SO_x , magnesium oxalate was selected as the precursor in the present study, which was pre-synthesized *via* a mild hydrothermal treatment of the $\text{MgC}_2\text{O}_4 \cdot 2\text{H}_2\text{O}$ polyhedrons derived from room temperature coprecipitation ⁴⁰. During the thermal conversion process, the nonionic surfactant nonyl phenol polyoxyethylene ether (NP-9) and NaCl were employed as the dispersing agent and flux, respectively. The successive and synergistic effect of NP-9 and NaCl favored the final formation of the high crystallinity porous MgO microrods, with a surface area of $50.20 \text{ m}^2 \text{ g}^{-1}$. Additionally, the as-obtained porous MgO microrods were used as high efficiency adsorbents for removal of heavy metal ions such as Pb (II) and Cr (VI) ions from aqueous solutions, indicating the present porous MgO microrods as promising cost effective candidates in the water treatment toward the increasingly focused environmental concerns nowadays.

2. Experimental

2.1. Room-temperature coprecipitation for $\text{MgC}_2\text{O}_4 \cdot 2\text{H}_2\text{O}$ microrods

All reagents were analytical grade and used as received without further purification. The precursor $\text{MgC}_2\text{O}_4 \cdot 2\text{H}_2\text{O}$ microrods were first synthesized *via* a facile hydrothermal treatment of the

MgC₂O₄·2H₂O polyhedrons, which were derived from a room temperature coprecipitation of sodium oxalate (Na₂C₂O₄) and magnesium chloride hexahydrate (MgCl₂·6H₂O), similar to that reported previously⁴⁰. In a typical procedure, keeping the molar ratio of MgCl₂ and Na₂C₂O₄ as 1 : 1, 25.0 mmol of Na₂C₂O₄ was dissolved into 25.0 mL of deionized (DI) water, then 12.0 mL of 2.08 mol L⁻¹ MgCl₂ solution and extra 3.0 mL of DI water was introduced successively under vigorous magnetic stirring. After stirring for 0.5 h at the room temperature, the resultant white slurry was transferred into a Teflon-lined stainless steel autoclave with a capacity of 67.0 mL. The autoclave was sealed, heated to 180 °C (heating rate: 5 °C min⁻¹), and then kept in an isothermal state for 3.0 h. After cooled down to room temperature naturally, the precursor was obtained after washed with DI water and absolute ethanol for three times and then filtered and finally dried at 70 °C for 6.0 h. In order to investigate the effect of the reaction temperature on the products, the temperature was tuned to room temperature, 60, and 120 °C, respectively, with other conditions unchanged.

2.2. Thermal conversion of MgC₂O₄·2H₂O to form porous MgO microrods

In the subsequent thermal conversion, 1.50 g of the as-obtained precursor MgC₂O₄·2H₂O microrods were ground with 30.0 mmol of NaCl and 8.0 mL of NP-9 for 5.0 and 30.0 min, respectively. The resultant slurry was transferred into a porcelain boat which was subsequently located in a horizontal quartz tube furnace, heated to 650 °C (heating rate: 10 °C min⁻¹) and kept in an isothermal state for 2.0 h. After the thermal conversion, the calcined samples were cooled down to room temperature naturally within the tube furnace, then collected and washed with DI water and absolute ethanol for three times, ultimately filtered and dried at 70 °C for 6.0 h. While to ascertain the specific effect of NaCl and NP-9, the calcination of the precursor only in the presence of NaCl or NP-9 was individually carried out at 650 °C within the tube furnace in an air atmosphere, with other conditions kept the same.

2.3. Removal of heavy metal Pb (II) and Cr (VI) ions

The as-obtained porous MgO microrods were evaluated for the removal of heavy metal ions of Pb (II) and Cr (VI) from aqueous solutions. In a typical procedure, for each system, 20.0 mg of MgO was dispersed into 20.0 mL of $\text{Pb}(\text{NO}_3)_2$ solution (concentration: 50.0 mg L^{-1}) under vigorous magnetic stirring at room temperature, with the stirring time ranging from 10.0 to 240.0 minutes. After the adsorption systems stirred for their designated time, the resultant slurry was filtered individually, leading to a series of transparent filtrate. The pH value of the filtrate was adjusted to 3.0 using HNO_3 (mass concentration: 10 %) so as to avoid the hydrolyzation and thus precipitation of Pb (II), and the filtrate was saved for measurement of the residual Pb^{2+} within the solution after adsorption by using the porous MgO microrods as adsorbent. In batch experiments for Cr (VI) adsorption, Cr (VI) solution with a concentration of 1.0 mg L^{-1} was prepared by dissolving specific amount of $\text{K}_2\text{Cr}_2\text{O}_7$ into proper volume of DI water. All of the Cr (VI) adsorption experiments were conducted by dispersing 20.0 mg of the as-obtained porous MgO microrods into 20.0 mL of the Cr (VI) solution under vigorous magnetic stirring at neutral pH, while with the stirring time ranging from 10.0 to 240.0 min. After the adsorption systems stirred for the designated time, the resultant slurry was filtered individually, resulting in a series of filtrate for further determination of the residual Cr (VI) within the solution after adsorption.

In order to investigate the composition change of the adsorbate, the filter cake was collected, washed with DI water and ethanol for three times, and dried at $70 \text{ }^\circ\text{C}$ for 6.0 h for characterization. For comparison of the adsorption efficiency, analytical grade of MgO reagent was also employed as so-called adsorbent, with other conditions kept the same.

2.4. Characterizations

The phase composition and structure of the samples were identified by an X-ray powder diffractometer (XRD, MiniFlux 600, Rigaku, Japan), using Cu-K α radiation ($\lambda = 1.54178 \text{ \AA}$) and a fixed power source (30.0 kV, 10.0 mA). The morphology and microstructure of the samples were examined by a field emission scanning electron microscopy (SEM, JSM 7401F, JEOL, Japan). The thermal decomposition behavior of the precursor was detected by a thermogravimetric analyzer (TGA, Netzsch STA 409C, Germany), carried out in dynamic air with a heating rate of $10 \text{ }^\circ\text{C min}^{-1}$. N $_2$ adsorption–desorption isotherms were measured at 77.3 K using a Chemisorption–Physisorption Analyzer (Autosorb-1-C, Quantachrome, USA). The specific surface area was calculated from the desorption branches in the relative pressure range of 0.05–0.30 using the multipoint Brunauer–Emmett–Teller (BET) method, the pore size distribution was evaluated from the N $_2$ desorption isotherm using the Barrett–Joyner–Halenda (BJH) method, and the total pore volume was calculated for pores with diameters less than a specific value of P/P_0 *ca.* 0.9896. While the actual residual amount of Pb $^{2+}$ within the solution was determined by an inductively coupled plasma mass spectrometry (ICP-MS) analysis (XSeries 2, Thermo Fisher, USA). The residual concentration of Cr (VI) in the supernatant solution after filtration was measured by diphenylcarbohydrazide method (Chinese GB 7466-87 and GB 7467-87) *via* a UV-vis spectrophotometer (UV-756CRT, Shanghai Yoke Instruments Meters Co., Ltd., China).

3. Results and Discussion

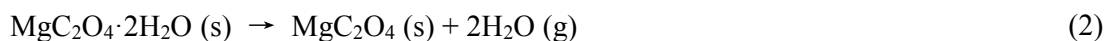
3.1. Hydrothermal formation of precursor MgC $_2$ O $_4$ ·2H $_2$ O microrods

The chemical constitution, morphology, and decomposition performance of the precursor microrods are showed in **Fig. 1**. Each diffraction peak of the precursor (**Fig. 1(a)**) was precisely indexed to that of the standard monoclinic MgC $_2$ O $_4$ ·2H $_2$ O (JCPDS No. 26-1223). The narrow and sharp

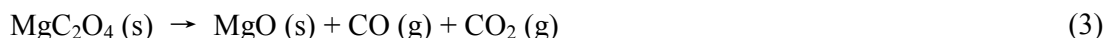
diffraction peaks indicated the high crystallinity of the precursor. This revealed the formation of the precursor $\text{MgC}_2\text{O}_4 \cdot 2\text{H}_2\text{O}$ *via* the following reaction:



The precursor exhibited rod-like morphology with distinct edges (**Fig.1(b)**), which was consistent with the sharp diffraction peaks demonstrated in the XRD pattern. The $\text{MgC}_2\text{O}_4 \cdot 2\text{H}_2\text{O}$ microrods had a length of 5.0-25.0 μm and a width of 1.0-4.0 μm . The thermal behavior of the $\text{MgC}_2\text{O}_4 \cdot 2\text{H}_2\text{O}$ precursor was investigated by the simultaneously recorded thermogravimetric-differential scanning calorimetry (TG-DSC) curves (**Fig. 1c**). The TG curve revealed that the sample mass decreased at a faster rate at 170-250 $^\circ\text{C}$, then abruptly dropped between 400 and 540 $^\circ\text{C}$, and finally remained almost constant thereafter. The former significant mass loss within 170-250 $^\circ\text{C}$ was *ca.* 23.05 %, similar to the theoretical value (24.32%) for the dehydration of $\text{MgC}_2\text{O}_4 \cdot 2\text{H}_2\text{O}$ to release two moles of crystal water as shown in eqn (2):



The latter abrupt mass loss within 400-540 $^\circ\text{C}$ was *ca.* 46.84 %, analogous to the theoretical value (48.65 %) for the thermal decomposition of the anhydrous MgC_2O_4 indicated by eqn (3):



Corresponding to the variation of the sample mass with the temperature, the simultaneously recorded DSC profile exhibited two distinct endothermic peaks at 170-250 and 400-540 $^\circ\text{C}$, attributed to the decomposition of the precursor within the two temperature ranges shown as eqn (2) and (3), respectively. The TG-DSC result suggested that the MgO phase could be available when the $\text{MgC}_2\text{O}_4 \cdot 2\text{H}_2\text{O}$ precursor was calcined above 540 $^\circ\text{C}$. The thermal decomposition behavior of the as-synthesized precursor $\text{MgC}_2\text{O}_4 \cdot 2\text{H}_2\text{O}$ microrods was quite similar to that of the previously obtained $\text{MgC}_2\text{O}_4 \cdot 2\text{H}_2\text{O}$ polyhedrons derived from room-temperature coprecipitation⁴⁰.

Fig. 2 displays the composition and morphology of the precursors synthesized at different temperatures with other parameters kept constant. Notably, with the temperature increasing from room temperature to 120 °C, detectable variation of the crystalline phase has emerged in the corresponding XRD patterns (**Fig. 2(a)**). The room temperature coprecipitation led to monoclinic glushinskite $\text{MgC}_2\text{O}_4 \cdot 2\text{H}_2\text{O}$ (JCPDS No. 28-0625) submicron polyhedrons (**Fig. 2(a,b)**) with a unit cell = $12.675 \times 5.406 \times 9.984 \text{ \AA}$, and the size was somehow smaller than that of we previously reported $\text{MgC}_2\text{O}_4 \cdot 2\text{H}_2\text{O}$ polyhedrons⁴⁰. When the temperature was increased to 60 °C, the product became short rod-like monoclinic $\text{MgC}_2\text{O}_4 \cdot 2\text{H}_2\text{O}$ (JCPDS No. 26-1223) micron particles with a unit cell = $12.689 \times 5.391 \times 9.977 \text{ \AA}$ (**Fig. 2(a,c)**). With the increase in the temperature from 60 to 120 °C, the length and aspect ratio of the rod-like micron particles became larger (**Fig. 2(a,d)**). Thus apparently, the hydrothermal treatment brought about the subtle conversion of the crystal structure of the precursor from $\text{MgC}_2\text{O}_4 \cdot 2\text{H}_2\text{O}$ (JCPDS No. 28-0625) submicron particles (**Fig. 2(b)**) to $\text{MgC}_2\text{O}_4 \cdot 2\text{H}_2\text{O}$ (JCPDS No. 26-1223) short rod-like micron particles (**Fig. 2(c)**) firstly, and then promoted the elongated or 1D preferential growth, leading to longer (**Fig. 2(d)**) and even higher aspect ratio (**Fig. 1(b)**) microrods thereafter.

3.2. Thermal conversion of precursor into porous MgO microrods

To improve the crystallinity of the product via the thermal conversion synthesis, the present precursor MgO microrods were calcined at a relatively high temperature as 650 °C. As shown in **Fig. 3**, after calcined for 2.0 h, all the products were readily indexed as the pure phase of periclase MgO (JCPDS No. 45-0946, **Fig. 3(a)**). With the introduction of onefold additive NaCl and even two kinds of additives NaCl and NP-9, the crystallinity of the calcined samples became higher and higher. When calcined in the absence of any additive, the products exhibited short rod-like micron and quasi irregular submicron particles (**Fig. 3(b)**). While calcined in the presence of NaCl, which

was used as high-temperature solvent elsewhere⁴¹, the product turned out to be tiny NPs (**Fig. 3(c)**). The key role of NaCl in improving the crystallinity of the calcined product here was analogous to that found in the flux assisted thermal conversion synthesis of pore-free Mg₂B₂O₅ nanowhiskers⁴².

Inspired by the striking effect of surfactants and molten salt on the preparation of the 1D metal oxides nanostructures with excellent morphology control^{43,44}, NaCl and NP-9 were employed in the thermal conversion of the present precursor for MgO as flux and surfactant, respectively. As shown in **Fig. 3(d)**, the product was found as well faceted microrods with some tiny NPs attached on the surfaces. The high magnification SEM image (**Fig. 3(d₁)**) clearly indicated the calcined MgO microrods of porous structure. The calcined porous MgO microrods have well retained the 1D morphology of the precursor MgC₂O₄·2H₂O microrods, and the mutual effect of NaCl and NP-9⁴⁰ on the morphology preservation was similar to that exhibited in formation of the peanut-shaped α-Fe₂O₃ structures⁴⁵ as well as rod-like Ni₃(BO₃)₂ particles⁴⁶.

The porous structure of the MgO microrods was further investigated by N₂ adsorption-desorption isotherms. As shown in **Fig. 3(e)**, the N₂ adsorption-desorption isotherms presented nearly type III characteristic with a hysteresis loop at a relative high pressure as P/P₀ = 0.84-1.0, revealing the existence of the mesoporous⁴⁷ and macroporous^{9,48} structure. The present N₂ sorption isotherms were similar to those of the porous MgO superstructures⁴⁰, and also analogous to those of the mesoporous MgO microspheres³⁹ and porous MgO nanoplates⁴⁹. Meanwhile, the pore size distribution (PSD, **Fig. 3(e₁)**) exhibited that the majority of the pores had a pore diameter of 8-50 nm, in addition to a few pores with the pore diameter less than 2 nm or larger than 50 nm. The PSD reconfirmed the as-obtained porous MgO microrods of hierarchical porous structures, ranging from micropores to mesopores and macropores. The multipoint BET was calculated as 50.2 m² g⁻¹, and this was a slightly smaller than that of MgO microspheres modified with ethylene glycol (55.9 m²

g^{-1})⁵⁰, whereas larger than that of the flower-like MgO ($45.0 \text{ m}^2 \text{ g}^{-1}$)⁵¹ obtained *via* an ethylene-glycol-mediated self-assembly process, and even larger than the double of that for the porous MgO superstructures⁴⁰. This revealed the abundant porosity in the porous MgO microrods.

3.3. Formation mechanism of porous MgO microrods

Based on the above room-temperature coprecipitation especially the hydrothermal conversion and calcination results, the formation mechanism of the present porous MgO microrods was inferred as **Fig. 4**. At room temperature first, the coprecipitation of Mg^{2+} and $\text{C}_2\text{O}_4^{2-}$ led to the nucleation and growth of $\text{MgC}_2\text{O}_4 \cdot 2\text{H}_2\text{O}$ (JCPDS No. 28-0625) submicron polyhedrons (**Fig. 4(a)**). Then the subsequent hydrothermal treatment promoted the crystalline structure conversion of $\text{MgC}_2\text{O}_4 \cdot 2\text{H}_2\text{O}$ (JCPDS No. 28-0625) polyhedrons, resulting in the hydrothermal formation of the precursor $\text{MgC}_2\text{O}_4 \cdot 2\text{H}_2\text{O}$ (JCPDS No. 26-1223) microrods (**Fig. 4(b)**) probably due to its intrinsic anisotropic crystal structure. This was similar to the hydrothermal growth of the 1D $\text{MgBO}_2(\text{OH})$ nanowhiskers without any additive⁵². During the calcination, the precursor $\text{MgC}_2\text{O}_4 \cdot 2\text{H}_2\text{O}$ microrods dehydrated and decomposed, and the released H_2O , CO as well as CO_2 gases led to hierarchical porous structure within the calcined microrods. Undoubtedly, the presence of NaCl and NP-9 was crucial for the preservation of the 1D morphology of the precursor microrods.

In our previous work, the thermal decomposition phenomena of NP-9 and also synergistic effect of NP-9 and NaCl on the formation of the well faceted hierarchical porous MgO superstructures was investigated in detail⁴⁰. Herein very similarly, although calcined at a temperature of $650 \text{ }^\circ\text{C}$ lower than its normal melting point (*ca.* $800 \text{ }^\circ\text{C}$), NaCl vapor could form⁴⁴ and then penetrate into and further migrate within the porous structure. The migrating NaCl vapor could serve as the gaseous flux, favoring the *in situ* crystallization and thus enhancement of the strength of the pore walls within the porous microrods. Consequently, the migrating gaseous flux strengthens the

toughness of the backbone and finally favors the preservation of the precursor's original microrod-like morphology. The similar key role of NaCl has also been confirmed in the NaCl assisted formation of the pore-free $\text{Mg}_2\text{B}_2\text{O}_5$ nanowhiskers *via* the thermal conversion of $\text{MgBO}_2(\text{OH})$ nanowhiskers at 650-700 °C⁴². And as a nonionic surfactant, NP-9 served as the dispersing agent and thus prevented the porous MgO particles from aggregating with each other (**Fig. 4c**). Consequently, it was the successive and synergistic effect of NaCl and NP-9 that gave rise to the final porous MgO microrods whereas with well faceted profile preserved. Notably, since the standard Gibbs free energy of formation of the $\text{MgC}_2\text{O}_4 \cdot 2\text{H}_2\text{O}$ precursor was not available at present, it was not likely to discuss the above formation mechanism from a pure thermodynamic point of view. However, it was not difficult to understand the thermodynamic feasibility for the whole process, taking the rapid room temperature coprecipitation of $\text{MgC}_2\text{O}_4 \cdot 2\text{H}_2\text{O}$ phase and its thermal decomposition at relatively high temperature to form porous MgO microrods.

3.4. MgO as adsorbents for removal of Pb (II) and Cr (VI) ions

Since the as-prepared hierarchical porous MgO microrods contained plenty of mesopores and macropores, the corresponding application as adsorbents for removal of lead (II) and chromium (VI) heavy metal ions was evaluated. **Fig. 5(a)** shows the adsorption rate of Pb (II) ion with an initial concentration of 50.0 mg L⁻¹. The adsorption process was very rapid during the first 30 min that the concentration of Pb (II) ion was decreased to 0.21 mg L⁻¹ at 10 min, and the equilibrium was established within 1.0 h. After 4.0 h, the concentration of Pb (II) ion was 0.15 mg L⁻¹. Correspondingly, the ratio of the concentration of Pb (II) at specific adsorption time to that of the original one decreased from 1.0 to 0.007 within 10 min, kept a slight dynamic vibration thereafter and reached equilibrium within 1.0 h. This indicated the adsorption efficiency has reached 99.3 % within 10 min, and ultimately remained relatively constant at 99.5 %. This was similar to 90-95 %

of EDTA-graphene oxide (initial concentration: 100 mg L^{-1})²⁷, whereas much higher than 70 % of the adsorbent Ca-montmorillonite (initial concentration: 58.79 mg L^{-1})⁵³ and 70 % of activated carbon-chitosan complex (initial concentration: 0.025 mol L^{-1})⁵⁴.

In order to better understand the present high adsorption efficiency, the XRD patterns of adsorbates were recorded (**Fig. 5(b₁)**). As shown, all the diffraction peaks could be assigned to MgO (JCPDS No. 45-0946), Mg(OH)₂ (JCPDS No. 07-0239) and Pb₃(CO₃)₂(OH)₂ (JCPDS No. 13-0131). The Mg(OH)₂ phase should be attributed to the hydration of MgO in aqueous solution. During the adsorption process, partially dissolved CO₂ reacted with MgO and Pb (II), producing Pb₃(CO₃)₂(OH)₂. In order to verify the reaction between MgO, CO₂ and Pb(II), commercial MgO reagent was also employed as adsorbent to undergo the same adsorption process, which also brought about the Pb₃(CO₃)₂(OH)₂ phase (**Fig. 5(b₂)**). Thus, the adsorption process was physical adsorption based on the hierarchical porous nature therein and the chemical adsorption, which was similar to the reaction between the flowerlike MgO and Pb (II) in the course of adsorption³⁰.

To further ascertain the formation of Pb₃(CO₃)₂(OH)₂ phase, extended experiments were carried out. However, where did carbonate come from or how was it formed was a hard nut to crack. Even the same adsorption test was performed in a strict N₂ protected system, the emergence of Pb₃(CO₃)₂(OH)₂ was also confirmed. Taking the basic groups on the surfaces of MgO and relative solubility of CO₂ in solution into account, the carbonate was probably derived from the adsorbed acidic CO₂ into the basic hierarchical porous MgO microrods from air and that dissolved into the solution. As known, the solubility product constant K_{sp} values of magnesium carbonate and lead carbonate were 3.5×10^{-8} and 7.4×10^{-14} , respectively. Although the K_{sp} of Pb₃(CO₃)₂(OH)₂ was not available at present, it was believed smaller than that of lead carbonate according to the experimental results, and also much smaller than that of magnesium carbonate. Thus, during the

adsorption process the adsorbed CO_2 within the porous MgO microrods and dissolved CO_2 within the solution might be released and reacted with Pb (II) under vigorous magnetic stirring, resulting in the $\text{Pb}_3(\text{CO}_3)_2(\text{OH})_2$ phase.

The as-obtained hierarchical porous MgO microrods were also employed as the adsorbents for removal of Cr (VI) (initial concentration: 1.0 mg L^{-1}), as shown in **Fig. 6 (a)**, with MgO reagent for comparison (**Fig. 6(b)**). Obviously, the as-obtained porous MgO microrods displayed higher adsorption efficiency than MgO reagent. About 30 % and 10 % of Cr (VI) was removed by 1.0 h of adsorption by using the as-obtained porous MgO microrods and MgO reagent as adsorbents, respectively. While after 4.0 h, the adsorption efficiencies was increased to 55.6 % and 20.7 %, respectively, indicating the significant effect of the hierarchical porous structures within the as-obtained MgO microrods on the adsorption of Cr (VI). The adsorption efficiency of Cr (VI) on the present hierarchical porous MgO microrods was lower than that on the maghemite (Fe_3O_4) NPs (58.9 %, pH = 2.5, initial concentration: 150 mg L^{-1})⁵⁵, whereas similar to that on the active carbon supported MgO micron particles (11.14 %, pH = 2, initial concentration: 50 mg L^{-1})⁵⁶, taking the difference of initial concentration employed into consideration. Notably however, the adsorption efficiency of Cr (VI) was not so remarkable compared with Pb (II). Under the aforesaid neutral pH condition, the degree of protonation of the porous MgO microrods' surface reduced gradually⁵⁷, while the dominant ionic form of Cr (VI) is dichromate ion ($\text{Cr}_2\text{O}_7^{2-}$ and other forms), and the abundance of OH^- ions increased the hindrance to diffusion of dichromate ions³⁷. After adsorption of Cr (VI), the adsorbates were confirmed as MgO (JCPDS No. 45-0946) and $\text{Mg}(\text{OH})_2$ (JCPDS No. 07-0239), and no Cr (VI) containing compounds were detected. This explained the relatively low adsorption efficiency of Cr (VI) by the present hierarchical porous MgO microrods, compared with the adsorption of Pb (II).

Although previous literatures showed that acid conditions were favorable for the removal of Cr (VI) ^{55, 56}, the neutral pH was employed when using pure porous MgO microrods as adsorbents. On one hand, distinct base condition will promote the transformation from MgO to Mg(OH)₂, which will definitely destroy the structure and further influence the recycling of the porous MgO microrods as adsorbents. On the other hand, distinct acid condition will favor the dissolution and further loss of MgO as adsorbents. Moreover, acid or base condition will exacerbate the impact to the environment. As a matter of fact, when the adsorption of Cr (VI) was performed within a different pH range of 2.0-8.0, the adsorption rate increased from 12% (pH=2.2) to 32% (pH=3.9) and then monotonously decreased to 2% (pH=8.0). Based on the adsorption performance at such a pH range and especially the impact to the environment, a neutral pH condition for the removal of Cr (VI) should be recommended. After all, the adsorption efficiency can be improved to some extent by using more inexpensive porous MgO microrods as adsorbents.

4. Conclusions

Hierarchical porous MgO microrods with a high crystallinity, well-defined rod-like morphology were obtained *via* a hydrothermal process (180 °C - 3.0 h) followed by a mild flux NaCl and surfactant NP-9 directed thermal conversion of the precursor at 650 °C. During the hydrothermal treatment, with the increase in the temperature, the room-temperature precipitate MgC₂O₄·2H₂O (JCPDS No. 28-0625) submicron polyhedrons were converted to MgC₂O₄·2H₂O (JCPDS No. 26-1223) firstly, and then the elongated or 1D preferential growth was promoted, leading to higher aspect ratio microrods. Within the subsequent thermal conversion, the successive and synergistic effect of NaCl and NP-9 played the key role in the final formation of the well-defined MgO microrods with a hierarchical porous structure (ranging from micropores to mesopores and macropores), specific surface area of 50.2 m² g⁻¹ and well preserved rod-like morphology of the

precursor $\text{MgC}_2\text{O}_4 \cdot 2\text{H}_2\text{O}$ microrods. The as-obtained hierarchical porous MgO microrods were utilized as efficient adsorbents for removal of heavy metal ions including Pb (II) and Cr (VI) from aqueous solutions, and the removal efficiency of Pb (II) (original concentration: 50.0 mg L^{-1}) and Cr (VI) (original concentration: 1.0 mg L^{-1}) was up to 99.5 % and 55.6 %, respectively. In addition to the present waste water treatment, the as-synthesized high crystallinity MgO microrods with hierarchical porous structure can also serve as alternative candidates for catalyst support and even catalyst itself in varieties of fields.

Acknowledgement

This work was supported by the National Natural Science Foundation of China (No. 21276141), the State Key Laboratory of Chemical Engineering, China (No. SKL-ChE-12A05). The authors also thank the reviewers for the constructive comments and suggestions on the improvement of the work.

References

1. A. Vantomme, A. Léonard, Z.-Y. Yuan and B.-L. Su, *Colloids Surf., A*, 2007, 300, 70-78.
2. K. Assaker, C. Carteret, P. Durand, L. Aranda, M. J. Stébé and J. L. Blin, *J. Phys. Chem. C*, 2013, 117, 16500-16508.
3. M. Q. Zhao, Q. Zhang, J. Q. Huang and F. Wei, *Adv. Funct. Mater.*, 2012, 22, 675-694.
4. L. H. Ai, H. T. Yue and J. Jiang, *Nanoscale*, 2012, 4, 5401-5408.
5. L.-R. Qin, J.-W. Zhao, L.-D. Zhang and X.-W. Zou, *Chem. Lett.*, 2006, 35, 380-381.
6. Y. Yan, L. Zhou and Y. Zhang, *J. Phys. Chem. C*, 2008, 112, 19831-19835.
7. X.-Y. Yu, T. Luo, Y. Jia, Y.-X. Zhang, J.-H. Liu and X.-J. Huang, *J. Phys. Chem. C*, 2011, 115, 22242-22250.
8. T.-Z. Ren, Z.-Y. Yuan and B.-L. Su, *Langmuir*, 2004, 20, 1531-1534.
9. P. Tian, J. Ye, G. Ning, W. Gong, N. Xu, Q. Zhang and Y. Lin, *RSC Advances*, 2012, 2, 10217-10221.
10. H. Bai, Z. Liu and D. D. Sun, *Chem. Asian J.*, 2012, 7, 1772-1780.

11. M. Abd-Ellah, N. Moghimi, L. Zhang, N. F. Heinig, L. Zhao, J. P. Thomas and K. T. Leung, *J. Phys. Chem. C*, 2013, 117, 6794-6799.
12. L. Xu, Q. Chen and D. Xu, *J. Phys. Chem. C*, 2007, 111, 11560-11565.
13. W. Zhu, X. Cui, X. Liu, L. Zhang, J.-Q. Huang, X. Piao and Q. Zhang, *Nanoscale Res Lett*, 2013, 8, 2.
14. W. Zhu, X. Cui, L. Wang, T. Liu and Q. Zhang, *Mater. Lett.*, 2011, 65, 1003-1006.
15. J. Liu, Jin Cheng, R. Che, J. Xu, Mengmei Liu and Z. Liu, *ACS Appl. Mater. Interfaces*, 2013, 5, 2503-2509.
16. Y. Li, X. Yan, W. Yan, X. Lai, N. Li, Y. Chi, Y. Wei and X. Li, *Chem. Eng. J.*, 2013, 232, 356-363.
17. T. Kathrina and R.D.Rawlings, *J. Mater. Sci.*, 1997, 32, 3951-3959.
18. M.-A. Faghihi-Sani and A. Yamaguchi, *Ceram. Int.*, 2002, 28, 835-839.
19. Q. Zhang, M. Zhao, J. Huang, W. Qian and F. Wei, *Chinese Journal of Catalysis*, 2008, 29, 1138-1144.
20. Q. Zhang, J.-Q. Huang, W.-Z. Qian, Y.-Y. Zhang and F. Wei, *Small*, 2013, 9, 1237-1265.
21. G. Zhao, J. Shi, G. Liu, Y. Liu, Z. Wang, W. Zhang and M. Jia, *J. Mol. Catal. A: Chem.*, 2010, 327, 32-37.
22. G. Moussavi and M. Mahmoudi, *Chem. Eng. J.*, 2009, 152, 1-7.
23. C. Gao, W. Zhang, H. Li, L. Lang and Z. Xu, *Cryst. Growth Des.*, 2008, 8, 3785-3790.
24. X. Sun, L. Yang, Q. Li, J. Zhao, X. Li, X. Wang and H. Liu, *Chem. Eng. J.*, 2014, 241, 175-183.
25. M. Eloussaief, W. Hamza, N. Kallel and M. Benzina, *Environmental Progress & Sustainable Energy*, 2013, 32, 229-238.
26. A. K. B. a, T. K. N. a, S. N. M. b and S. K. Das, *Chem. Eng. J.*, 2008, 137, 529-541.
27. C. J. Madarang, H. Y. Kim, G. Gao, N. Wang, J. Zhu, H. Feng, M. Gorring, M. L. Kasner and S. Hou, *ACS Appl. Mater. Interfaces*, 2012, 4, 1186-1193.
28. J. Hu, Z. Song, L. Chen, H. Yang, J. Li and R. Richards, *J. Chem. Eng. Data*, 2010, 55, 3742-3748.
29. T. G. Venkatesha, R. Viswanatha, Y. Arthoba Nayaka and B. K. Chethana, *Chem. Eng. J.*, 2012, 198-199, 1-10.
30. C.-Y. Cao, J. Qu, F. Wei, H. Liu and W.-G. Song, *ACS Appl. Mater. Interfaces*, 2012, 4,

- 4283-4287.
31. Z. Zhao, H. Dai, Y. Du, J. Deng, L. Zhang and F. Shi, *Mater. Chem. Phys.*, 2011, 128, 348-356.
 32. Y. Liu, Q. Li, S. Gao and J. K. Shang, *J. Am. Ceram. Soc.*, 2011, 94, 217-223.
 33. B. Huo, L. Hu, H. Zhang, Q. Fu, J. Zhu and X. Chen, *Micro & Nano Letters*, 2009, 4, 59-62.
 34. M. Sharma and P. Jeevanandam, *J. Alloys Compd.*, 2011, 509, 7881-7885.
 35. N. Sutradhar, A. Sinhamahapatra, S. K. Pahari, P. Pal, H. C. Bajaj, I. Mukhopadhyay and A. B. Panda, *J. Phys. Chem. C*, 2011, 115, 12308-12316.
 36. J. C. Yu, A. Xu, L. Zhang, R. Song and L. Wu, *J. Phys. Chem. B*, 2004, 108, 64-70.
 37. R. Hahn, J. G. Brunner, J. Kunze, P. Schmuki and S. Virtanen, *Electrochem. Commun.*, 2008, 10, 288-292.
 38. Y. Ding, G. Zhang, H. Wu, B. Hai, L. Wang and Y. Qian, *Chem. Mater.*, 2001, 13, 435-440.
 39. J. Zhou, S. Yang and J. Yu, *Colloids Surf., A*, 2011, 379, 102-108.
 40. W. Zhu, L. Zhang, Gui-Li Tian, R. Wang, H. Zhang, X. Piao and Q. Zhang, *CrystEngComm*, 2014, 16, 308-318.
 41. A. L. Tiano, A. C. Santulli, C. Koenigsmann, M. Feygensohn, M. C. Aronson, R. Harrington, J. B. Parise and S. S. Wong, *Chem. Mater.*, 2011, 23, 3277-3288.
 42. W. C. Zhu, Q. Zhang, L. Xiang and S. L. Zhu, *Cryst. Growth Des.*, 2011, 11, 709-718.
 43. W. Wang and L. Ao, *Cryst. Growth Des.*, 2008, 8, 358-362.
 44. P. M. Rørvik, T. Lyngdal, R. Sæterli, A. T. J. v. Helvoort, R. Holmestad, T. Grande and Mari-Ann Einarsrud*, *Inorg. Chem.*, 2008, 47, 3173-3181.
 45. T.-J. Park and S. S. Wong, *Chem. Mater.*, 2006, 18, 5289-5295.
 46. X. Liu, W. Zhu, X. Cui, T. Liu and Q. Zhang, *Powder Technol.*, 2012, 222, 160-166.
 47. J. Lian, C. Zhang, P. Wang and D. H. L. Ng, *Chem. Asian J.*, 2012, 7, 2650-2655.
 48. F. Mou, J. Guan, H. Ma, L. Xu and W. Shi, *ACS Appl. Mater. Interfaces*, 2012, 4, 3987-3993.
 49. H. X. Niu, Q. Yang, K. B. Tang and Y. Xie, *Microporous Mesoporous Mater.*, 2006, 96, 428-433.
 50. J. Jin, Z. Zhang, H. Ma, X. Lu, J. Chen, Q. Zhang, H. Zhang and Y. Ni, *Mater. Lett.*, 2009, 63, 1514-1516.
 51. S. W. Bain, Z. Ma, Z. M. Cui, L. S. Zhang, F. Niu and W. G. Song, *J. Phys. Chem. C*, 2008,

- 112, 11340-11344.
52. W. C. Zhu, S. L. Zhu and L. Xiang, *CrystEngComm*, 2009, 11, 1910-1919.
53. Y. Li, J. Wang, X. Wang and J. Wang, *Ind. Eng. Chem. Res.*, 2012, 51, 6520-6528.
54. H. Ge and X. Fan, *Chem. Eng. Technol.*, 2011, 34, 1745-1752.
55. J. Hu, G. Chen and I. M. C. Lo, *Water Res.*, 2005, 39, 4528-4536.
56. K. Peng, Z. Jia, R. Zhu and J. Zhou, *Journal of The Chinese Ceramic Society*, 2011, 39, 1651-1658.
57. M. Kobya, *Bioresour. Technol.*, 2004, 91, 317-321.

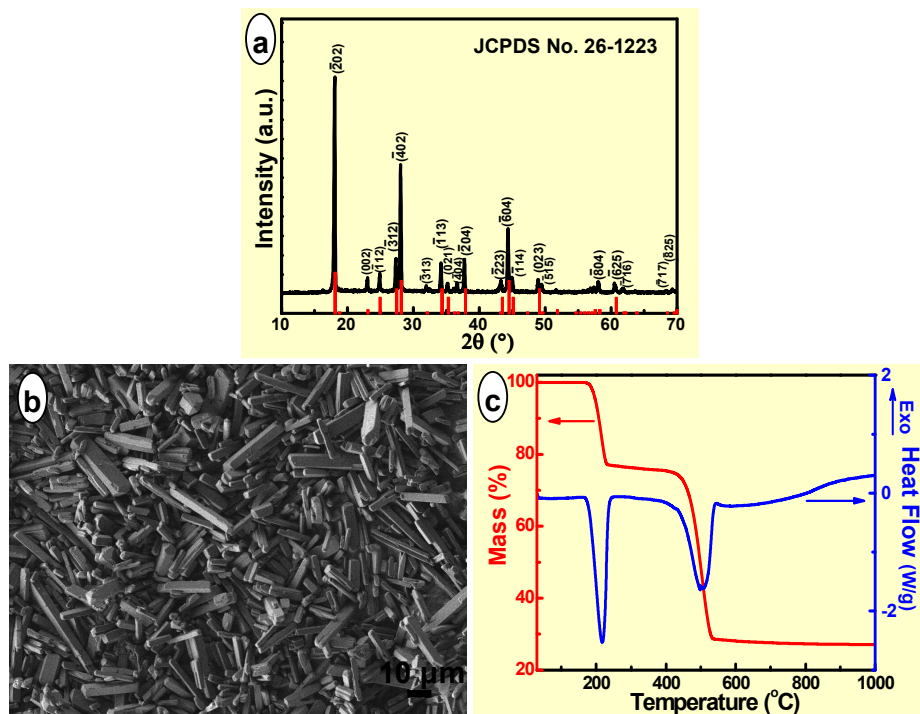


Fig. 1. (a) XRD pattern, (b) SEM image and (c) TG-DSC curves of the precursor $\text{MgC}_2\text{O}_4 \cdot 2\text{H}_2\text{O}$ microrods hydrothermally synthesized at 180 $^{\circ}\text{C}$ for 3.0 h.

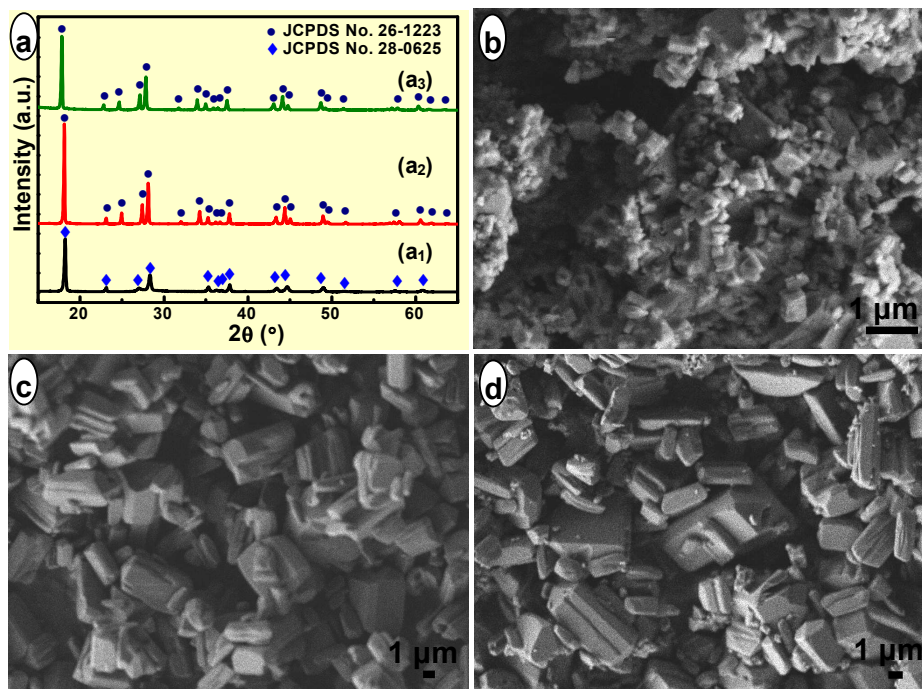


Fig. 2. (a) XRD patterns and (b-d) SEM images of the precursor $\text{MgC}_2\text{O}_4 \cdot 2\text{H}_2\text{O}$ microrods hydrothermally synthesized at different temperatures for 3.0 h. Temperature ($^{\circ}\text{C}$): (a₁,b)-room temperature; (a₂,c)-60; (a₃, d)-120.

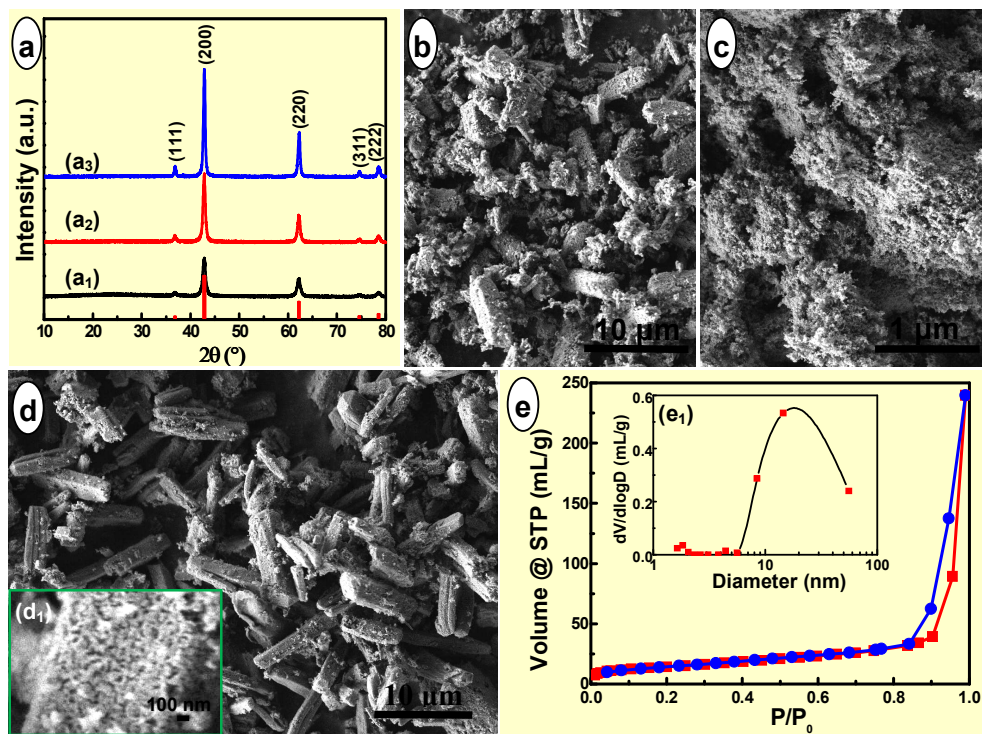


Fig. 3. (a) XRD patterns, (b-d) SEM images, and (e) N₂ adsorption-desorption isotherms of the products calcined from the precursor in the (a₁, b) absence, or (a₂, c) presence of NaCl, as well as (a₃, d, e, e₁) NaCl and NP-9 at 650 °C for 2.0 h. Inset (e₁) was the corresponding pore size distribution.

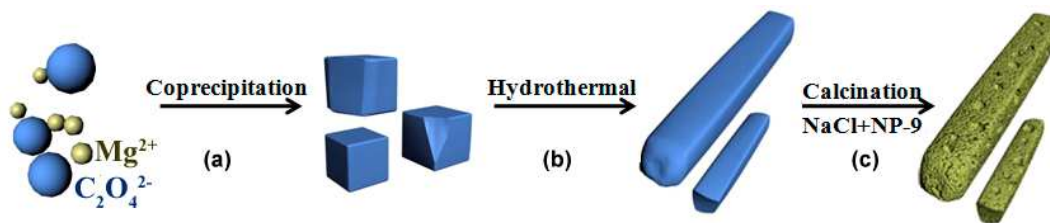


Fig. 4. The proposed formation mechanism of the hierarchical porous MgO microrods. (a) Room-temperature coprecipitation of Mg^{2+} and $C_2O_4^{2-}$ resulted in the nucleation and growth of $MgC_2O_4 \cdot 2H_2O$ polyhedrons; (b) Hydrothermal treatment of the $MgC_2O_4 \cdot 2H_2O$ polyhedrons at 180 °C for 3.0 h led to $MgC_2O_4 \cdot 2H_2O$ microrods; (c) NaCl and NP-9 assisted thermal conversion of the $MgC_2O_4 \cdot 2H_2O$ microrods at 650 °C for 2.0 h gave rise to porous MgO microrods.

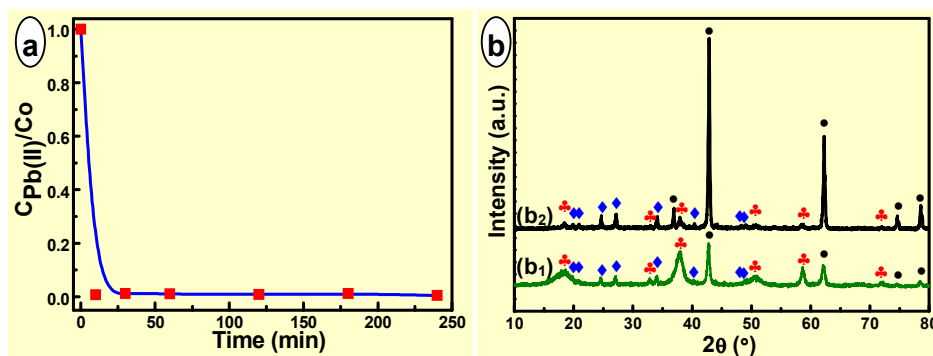


Fig. 5. (a) The adsorption of Pb (II) and (b) the compositions of adsorbates after adsorption, using (a, b₁) the as-synthesized hierarchical porous MgO microrods as adsorbent and (b₂) MgO reagent for comparison. Initial concentration (mg L⁻¹): Pb (II)-50.0.

● MgO (JCPDS No. 45-0946), ♣ Mg(OH)₂ (JCPDS No. 07-0239), ◆ Pb₃(CO₃)₂(OH)₂ (JCPDS No. 13-0131).

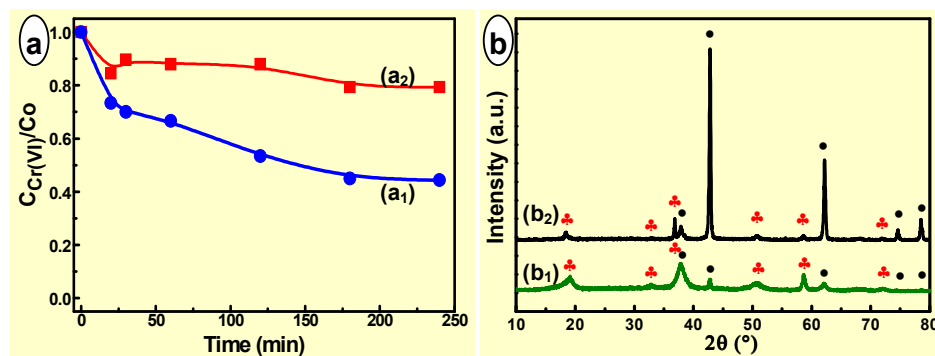


Fig. 6. (a) The adsorption of Cr (VI) and (b) compositions of the adsorbates after adsorption, using (a₁,b₁) the as-synthesized hierarchical porous MgO microrods as adsorbents and (a₂, b₂) MgO reagent for comparison. Initial concentration (mg L⁻¹): Cr (VI)-1.0.

- MgO (JCPDS No. 45-0946), ♣ Mg(OH)₂ (JCPDS No. 07-0239).